Journal of Biomedical Optics

SPIEDigitalLibrary.org/jbo

Oxygen tomography by Čerenkov-excited phosphorescence during external beam irradiation

Rongxiao Zhang
Scott C. Davis
Jennifer-Lynn H. Demers
Adam K. Glaser
David J. Gladstone
Tatiana V. Esipova
Sergei A. Vinogradov
Brian W. Pogue

SPIE

Oxygen tomography by Čerenkov-excited phosphorescence during external beam irradiation

Rongxiao Zhang,[a*] Scott C. Davis,[b*] Jennifer-Lynn H. Demers,[b] Adam K. Glaser,[b] David J. Gladstone,[c,d] Tatiana V. Esipova,[e] Sergei A. Vinogradov,[e] and Brian W. Pogue[a,b,d]
[a]Dartmouth College, Department of Physics and Astronomy, Hanover, New Hampshire 03755
[b]Dartmouth College, Thayer School of Engineering, Hanover, New Hampshire 03755
[c]Dartmouth College, Department of Medicine, Geisel School of Medicine, Hanover, New Hampshire 03755
[d]Norris Cotton Cancer Center, Dartmouth-Hitchcock Medical Center, Lebanon, New Hampshire 03766
[e]University of Pennsylvania, Department of Biochemistry and Biophysics, Perelman School of Medicine, Philadelphia, Pennsylvania 19104

Abstract. The efficacy of radiation therapy depends strongly on tumor oxygenation during irradiation. However, current techniques to measure this parameter *in vivo* do not facilitate routine monitoring in patients. Herein, we demonstrate a noninvasive method for tomographic imaging of oxygen partial pressure (pO_2) in deep tissue using the phosphorescence decay of an oxygen-sensitive probe excited by Čerenkov radiation induced by external beam radiotherapy. Tissue-simulating scattering phantoms (60 mm diameter with a 20 mm anomaly) containing platinum(II)-G4 (PtG4), a dendritic porphyrin-based phosphor, whose phosphorescence is quenched in the presence of oxygen, were irradiated with a clinical linear accelerator. The emitted phosphorescence was measured at various positions on the phantom boundary using a spectrograph coupled to an intensified charge-coupled device (ICCD). At each position, PtG4 phosphorescence decay curves were measured by synchronizing the ICCD to the linear accelerator pulses. Tomographic images of phosphorescence yield and lifetime were recovered for phantoms with homogenous PtG4 concentrations and heterogeneous pO_2. Since PtG4 lifetime is strongly and predictably dependent on pO_2 through the Stern-Volmer relationship, tomographic images of pO_2 were also reported, and showed excellent agreement with independent oxygenation measurements. Translating this approach to the clinic could facilitate direct sensing of pO_2 during radiotherapy. [DOI: 10.1117/1.JBO.18.5.050503]

Keywords: Čerenkov; phosphorescence; optics tomography; oxygen partial pressure; LINAC; time domain gating; external beam radiotherapy.

Paper 130023LR received Jan. 16, 2013; revised manuscript received Apr. 3, 2013; accepted for publication Apr. 9, 2013; published online May 3, 2013.

*Authors contributed equally to this work.

Address all correspondence to: Brian W. Pogue, Dartmouth College, Department of Physics and Astronomy, Hanover, New Hampshire 03755. Tel: +603 646-3861; Fax: +603 646-3856; E-mail: brian.w.pogue@dartmouth.edu

Tissue oxygenation is a major factor influencing the success or failure of radiation therapy.[1] Thus, techniques for measuring tumor partial pressure of oxygen (pO_2) during the daily fractions of radiation therapy given to patients could be extremely useful for tuning treatment conditions and monitoring therapeutic outcome. However, most methods to measure pO_2 in tissue require invasive instruments[2] and thus are difficult to repeat daily and are sensitive to the high microscopic heterogeneity of pO_2 in tumors.[3] An alternative, noninvasive imaging approach using oxygen-dependent quenching of phosphorescence has been shown to provide accurate images of pO_2 in tumor tissues in planar[4] and tomographic[5] imaging geometries. The phosphorescence lifetime of these probes is a robust and sensitive indicator of pO_2 in the environment. Applying this noninvasive approach during radiation therapy could enable monitoring of tissue oxygenation during the entire course of treatment, allowing assessment and dose optimization throughout the regimen.

The occurrence of Čerenkov radiation in tissue during external beam radiotherapy (EBRT) has been demonstrated in several recent papers.[6–7] Measuring this emission, as well as secondary luminescence of a fluorophore or phosphor excited by the Čerenkov radiation, i.e., Čerenkov radiation excited luminescence (CREL), has potential for monitoring a variety of functional parameters during radiation therapy. Previously, we demonstrated that phosphorescence of a near-infrared (NIR) oxygen-sensitive probe [platinum(II)-G4, PtG4][7,8] can be excited by Čerenkov emission and measured EBRT in tissue phantoms[7] in a point-probe geometry. Coupling this measurement approach with a tomographic imaging modality would facilitate volumetric assessment of tissue oxygenation and provide more accurate quantification of these parameters in deep tissues. In this letter, we investigate the ability to recover tomographic images of CREL-induced phosphorescence yield in a variety of phantom configurations and oxygenations states, and examine the feasibility of CREL tomography to recover images of pO_2 from time-resolved phosphorescence measurements.

The experimental configuration is shown in Fig. 1(a). The external beam irradiator was a Varian Clinic 2100CD linear accelerator (LINAC). In this study, the LINAC was set to irradiate the phantom with a 4-cm-square gamma photon beam with energy of 6 MV and a dose rate of 600 MU/min. A 60-mm-diameter cylindrical tissue-simulating phantom was positioned on the treatment bed 100 cm from the LINAC head. The phantom contained a 20-mm-diameter cylindrical anomaly region to simulate tumor tissue. Both the background and anomaly were filled with 1% v/v intralipid emulsion in water to mimic tissue properties for both external beam radiation and optical photon propagation. In addition to the water/intralipid solution, PtG4, the oxygen-sensitive phosphor, was added to the background and anomaly regions of the phantom. Oxygen quenches the phosphorescence emission and lengthens the phosphorescence lifetime of this probe in a well-defined way, making PtG4 a reliable reporter of pO_2. Four combinations of PtG4 contrast and oxygenation states were used, as tabulated in Fig. 2. Oxygenation in the anomaly was controlled using the glucose/glucose oxidase/catalase system. Reference values for the PtG4 phosphorescence lifetime in deoxygenated and oxygenated environments were measured independently using a frequency-domain phosphorometer.[9]

Optical measurements were acquired with a gated Princeton Instruments PI-MAX3 ICCD attached to an Acton Research

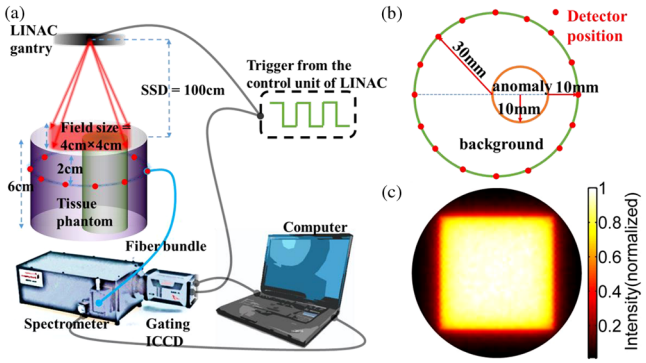

Fig. 1 (a) Diagram of the measurement system consisting of a linear accelerator, radiation/optical tissue phantom, and an optical fiber that couples light from the phantom to a spectrometer with a gated ICCD synchronized to the radiation bursts of the LINAC. (b) Top view of the phantom geometry. (c) A two-dimensional cross-section of the Čerenkov field modeled using Geant4-based architecture for machine-oriented simulations (GAMOS) and used as the excitation field for phosphorescence yield image reconstruction.

Insight spectrograph positioned outside the treatment room. The ICCD was cooled to −25°C and the intensifier set to the maximum gain. Light emitted from the phantom was coupled to the spectrometer through a fiber bundle composed of nineteen 200-μm silica fibers. Using a gated ICCD enables the system to take advantage of the pulsed operation of LINACs. Radiation from the LINAC is delivered in 3.23 μs bursts at a repetition rate of 200 Hz. By synchronizing the ICCD with a trigger signal from the LINAC, as described previously,[7,10] the intensity of CREL at different time points after each radiation burst can be measured. This effectively eliminates the contaminating excitation signal, i.e., the Čerenkov emission itself, and facilitates the measurement of phosphorescence lifetime.

In this study, optical measurements were acquired after the radiation pulses at time delays between 0 and 200 μs in 4 μs increments, with a gate width of 500 μs. To improve signal-to-noise, 100 spectra were acquired at each time delay and summed up. Background measurements were also acquired and subtracted from the spectra. To produce a full tomographic data set, this process was repeated (sequentially) for 16 positions of the fiber bundle around the boundary of the phantom as represented in Fig. 1(a) and 1(b). Once processed, all spectra were reduced to a single intensity value suitable for image reconstruction by integrating ±50 nm around the PtG4 phosphorescence peak $\lambda_{max} = 772$ nm.

Reconstructing images of phosphorescence yield requires an estimate of the optical excitation field, which in this case is the Čerenkov field. Accurate modeling of the Čerenkov field can be accomplished by employing established tools from radiation oncology. In this study, GAMOS (Geant4-based Architecture for Medicine-Oriented Simulations)[11]was used to simulate a 6 MV gamma photon beam, irradiating a 6×6 cm^2 area with voxel size 0.5 mm × 0.5 mm × 0.5 mm. A total of 10^7 primary particles were launched, and the Čerenkov photons generated were scored.[7] A two-dimensional slice of the field, corresponding to the plane of the optical detectors, was extracted and adopted as the excitation field for image reconstruction.

The excitation field and processed optical data from the CREL measurements were combined to recover images of phosphorescence yield using the fluorescence toolbox in NIRFAST,[12,13] a finite element-based software package for diffusion-based NIR image reconstruction. Images were recovered using a 60-mm-diameter mesh with 1785 nodes, homogeneous absorption (μ_a) and scattering (μ'_s) properties at the excitation ($\mu'_{ax} = 0.033$ mm^{-1}, $\mu'_{sx} = 1.8$ mm^{-1}) and emission ($\mu_{am} = 0.002$ mm^{-1}, $\mu'_{sm} = 1.033$ mm^{-1}) wavelengths, and a refractive index $n = 1.327$.

To demonstrate external beam-induced CREL tomography of PtG4, reconstructions were performed in the four phantom configurations using a time delay of zero with respect to the falling edge of the radiation burst, which is simply the integrated phosphorescence decay after the pulse. Images of phosphorescence yield and the associated recovered contrast values, calculated as the mean phosphorescence yield in the known area of interest divided by the same in the known background area, are presented in Fig. 2. These results closely follow expected trends, with the deoxygenated region producing the highest phosphorescence yields and contrasts. Particularly encouraging are the images for phantoms with a constant concentration of PtG4 in both the background and tumor region. While clear contrast in phosphorescence yield was observed when the phantom contained an anoxic tumor region, a nearly homogenous distribution was obtained when both regions were aerated. This demonstrates the strong sensitivity of PtG4 CREL tomography to PO_2, and insensitivity to phosphor concentration.

To examine the feasibility of using this imaging approach for CREL-based pO_2 tomography during radiation therapy, time-resolved phosphorescence decay images were analyzed for the phantom with a constant concentration of PtG4 but with an aerated background and anoxic tumor region, as may be encountered *in vivo*. This was accomplished by reconstructing images for each time delay (from 0 to 200 μs in 4 μs increments) and fitting each image pixel over time to a single exponential [Eq. (1)]:

$$I_t = I_0 \tau \exp\left(\frac{-t}{\tau}\right), \tag{1}$$

where I_0 is the decay initial intensity, I_t is the intensity measured for different time points, and τ is the phosphorescence lifetime. Figure 3(a) shows the phosphorescence decay curves for pixels in the anoxic and aerated regions, labeled Anomaly and Background, respectively. The full image of phosphorescence lifetime is shown in Fig. 3(b). From this image, an image of pO_2 can be recovered directly using the Stern-Volmer equation, which relates lifetime and pO_2.

$$\frac{1}{\tau} = \frac{1}{\tau_0} + k_q \times pO_2, \tag{2}$$

where τ is phosphorescence lifetime, τ_0 is the lifetime in the absence of oxygen ($pO_2 = 0$, and k_q is the oxygen quenching constant.

The resulting pO_2 image is shown in Fig. 3(c). It is noteworthy that the recovered values of pO_2 in the aerated (150 Torr

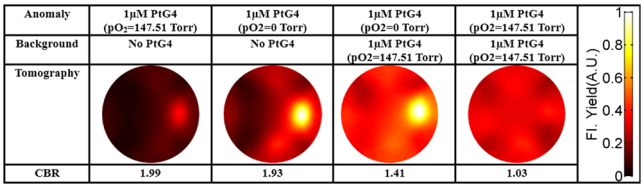

Fig. 2 Images of phosphorescence yield from CREL tomography and associated contrast-to-background values for four PtG4 phantom configurations.

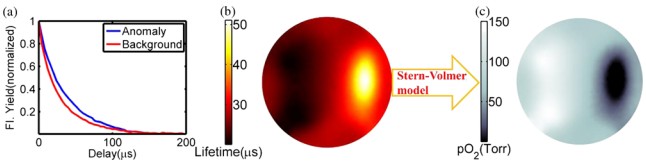

Fig. 3 (a) Phosphorescence decays calculated as the average values in the aerated anomaly and anoxic background. (b) Recovered lifetime distribution. (c) pO_2 distribution converted from the lifetime distribution using the Stern-Volmer model.

approximately) and anoxic regions (0 Torr approximately) are very close to the true values measured with the reference probe (reported in Fig. 2). Furthermore, images of pO_2 and lifetime provide much higher contrasts than those of phosphorescence yield alone, suggesting that the time-dependent approach is more sensitive and quantitative than imaging based on intensity alone.

These results suggest that CREL-based oxygen tomography is feasible and that incorporating time-domain analysis can provide an accurate, robust, and quantitative pO_2 imaging paradigm. The delivery of megavoltage radiotherapy is well controlled and extensively planned for each subject and Čerenkov radiation emission will be emitted from targeted cancer tissues where the charged primary or secondary particles deposit most of their energy. Thus, CREL will often be excited in rather deep tissue regions. The emission peaks of the oxygen-sensitive phosphors are well above 750 nm and thus propagate readily through most tissues. Standard diffuse optical tomography (DOT) systems commonly measure light at these wavelengths through 10 cm of tissue without requiring invasive placement of the optical detectors. As in all forms of optical NIR tomography, tissue scattering and absorption limit depth resolution of the disclosed method. However, because of the relatively slow time scale of triplet emission, phosphorescence lifetime imaging is less affected by scattering and absorption[14] than, e.g., fluorescence lifetime imaging, allowing for more accurate spatial reconstructions.

The image quality of the tomograms is consistent with typical DOT images, which are generally of low-spatial resolution. However, the prevailing trend in DOT is the implementation of spatial priors from conventional imaging modalities. Since all patients undergoing EBRT also have extensive co-registered CT scans used for treatment planning, one could envision using these data to guide the recovery of pO_2. While total acquisition times reported here were rather long (about 25 s per position), the instrument and experimental procedure used in this proof-of-concept study were not optimized for fast acquisition. Small-diameter fibers and single-channel spectroscopic detection were all unnecessary constraints limiting acquisition speed. Large-diameter fiber bundles and coupled to gated wide-area avalanche photodiodes or photomultiplier tubes could improve light collection efficiency by over 1500-fold without loss of image quality. Additional improvements in signal intensity would obtain using more optimized oxygen-sensitive probes at higher concentrations, as have been studied previously.[8]

The ability to image pO_2 distribution during radiotherapy, as demonstrated here, would provide unprecedented information about the tumor micro-environment. This may have a significant impact in radiotherapy research programs, such as in the development of adjuvant and synergistic therapies, and in planning and tailoring clinical treatment regimens.

Acknowledgments

This work was supported by NIH grants R01CA120368 (BWP), R01CA109558 (BWP) and Department of Defense award W81XWH-09-1-0661 (SCD). SAV acknowledges support of the grant from the Penn Comprehensive Neuroscience Center.

References

1. P. Vaupel, A. Mayer, and M. Hockel, "Impact of hemoglobin levels on tumor oxygenation: the higher, the better?," *Strahlentherapie Und Onkologie* **182**(2), 63–71 (2006).
2. M. Nordsmark et al., "Measurements of hypoxia using pimonidazole and polarographic oxygen-sensitive electrodes in human cervix carcinomas," *Radiother. Oncol.* **67**(1), 35–44 (2003).
3. S. M. Evans and C. J. Koch, "Prognostic significance of tumor oxygenation in humans," *Cancer Lett.* **195**(1), 1–16 (2003).
4. D. F. Wilson and G. J. Cerniglia, "Localization of tumors and evaluation of their state of oxygenation by phosphorescence imaging," *Cancer Res.* **52**(14), 3988–3993 (1992).
5. S. V. Apreleva, D. F. Wilson, and S. A. Vinogradov, "Tomographic imaging of oxygen by phosphorescence lifetime," *Appl. Opt.* **45**(33), 8547–8559 (2006).
6. J. Axelsson et al., "Cerenkov emission induced by external beam radiation stimulates molecular fluorescence," *Med. Phys.* **38**(7), 4127–4132 (2011).
7. R. Zhang et al., "Cerenkov radiation emission and excited luminescence (CREL) sensitivity during external beam radiation therapy: Monte Carlo and tissue oxygenation phantom studies," *Biomed. Opt. Express* **3**(10), 2381–2394 (2012).
8. T. V. Esipova et al., "Two new "protected" oxyphors for biological oximetry: properties and application in tumor imaging," *Anal. Chem.* **83**(22), 8756–8765 (2011).
9. S. A. Vinogradov et al., "Frequency domain instrument for measuring phosphorescence lifetime distributions in heterogeneous samples," *Rev. Sci. Instrum.* **72**(8), 3396–3406 (2001).
10. A. K. Glaser et al., "Time-gated Cherenkov emission spectroscopy from linear accelerator irradiation of tissue phantoms," *Opt. Lett.* **37**(7), 1193–1195 (2012).
11. P. Arce, P. R. Mendes, and J. I. Lagares"GAMOS: an Easy and Flexible Framework for Geant4 Simulations," in *2008 IEEE Proc. Nuc. Sci. Symp. Conf. Rec.*, pp. 3162–3168 (2008).
12. S. C. Davis et al., "Image-guided diffuse optical fluorescence tomography implemented with Laplacian-type regularization," *Opt. Express* **15**(7), 4066–4082 (2007).
13. H. Dehghani et al., "Near infrared optical tomography using NIRFAST: Algorithm for numerical model and image reconstruction," *Commun. Numer. Methods Eng.* **25**(6), 711–732 (2009).
14. S. V. Apreleva and S. A. Vinogradov, "Influence of optical heterogeneities on reconstruction of spatial phosphorescence lifetime distributions," *Opt. Lett.* **33**(8), 782–784 (2008).